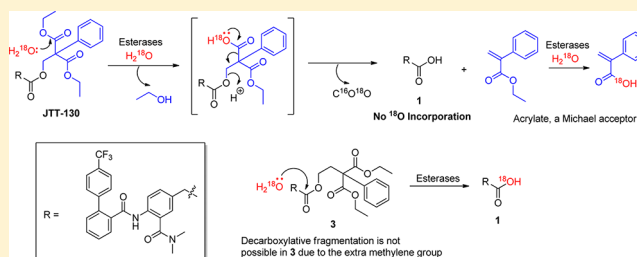


## Insights into the Novel Hydrolytic Mechanism of a Diethyl 2-Phenyl-2-(2-arylacetoxy)methyl Malonate Ester-Based Microsomal Triglyceride Transfer Protein (MTP) Inhibitor

Tim Ryder,<sup>†</sup> Gregory S. Walker,<sup>†</sup> Theunis C. Goosen,<sup>†</sup> Roger B. Ruggeri,<sup>‡</sup> Edward L. Conn,<sup>§</sup> Benjamin N. Roche,<sup>§</sup> Kimberly Lapham,<sup>†</sup> Claire M. Steppan,<sup>†</sup> David Hepworth,<sup>‡</sup> and Amit S. Kalgutkar<sup>\*,||</sup><sup>†</sup>Pharmacokinetics, Dynamics, and Metabolism—New Chemical Entities, Pfizer Worldwide Research and Development, Groton, Connecticut 06340, United States<sup>‡</sup>Cardiovascular Metabolic and Endocrine Diseases Medicinal Chemistry, Pfizer Worldwide Research and Development, Cambridge, Massachusetts 02139, United States<sup>§</sup>Cardiovascular Metabolic and Endocrine Diseases Medicinal Chemistry, Pfizer Worldwide Research and Development, Groton, Connecticut 06340, United States<sup>||</sup>Pharmacokinetics, Dynamics, and Metabolism—New Chemical Entities, Pfizer Worldwide Research and Development, Cambridge, Massachusetts 02139, United States

## S Supporting Information

**ABSTRACT:** Inhibition of intestinal and hepatic microsomal triglyceride transfer protein (MTP) is a potential strategy for the treatment of dyslipidemia and related metabolic disorders. Inhibition of hepatic MTP, however, results in elevated liver transaminases and increased hepatic fat deposition consistent with hepatic steatosis. Diethyl 2-((2-(3-(dimethylcarbamoyl)-4-(4'-(trifluoromethyl)-[1,1'-biphenyl]-2-ylcarboxamido)-phenyl)acetoxy)methyl)-2-phenylmalonate (JTT-130) is an intestine-specific inhibitor of MTP and does not cause increases in transaminases in short-term clinical trials in patients with dyslipidemia. Selective inhibition of intestinal MTP is achieved via rapid hydrolysis of its ester linkage by liver-specific carboxylesterase(s), resulting in the formation of an inactive carboxylic acid metabolite **1**. In the course of discovery efforts around tissue-specific inhibitors of MTP, the mechanism of JTT-130 hydrolysis was examined in detail. Lack of <sup>18</sup>O incorporation in **1** following the incubation of JTT-130 in human liver microsomes in the presence of H<sub>2</sub><sup>18</sup>O suggested that hydrolysis did not occur via a simple cleavage of the ester linkage. The characterization of atropic acid (2-phenylacrylic acid) as a metabolite was consistent with a hydrolytic pathway involving initial hydrolysis of one of the pendant malonate ethyl ester groups followed by decarboxylative fragmentation to **1** and the concomitant liberation of the potentially electrophilic acrylate species. Glutathione conjugates of atropic acid and its ethyl ester were also observed in microsomal incubations of JTT-130 that were supplemented with the thiol nucleophile. Additional support for the hydrolysis mechanism was obtained from analogous studies on diethyl 2-(2-(2-(3-(dimethylcarbamoyl)-4-(4'-trifluoromethyl)-[1,1'-biphenyl]-2-ylcarboxamido)phenyl)acetoxy)ethyl)-2-phenylmalonate (**3**), which cannot participate in hydrolysis via the fragmentation pathway because of the additional methylene group. Unlike the case with JTT-130, <sup>18</sup>O was readily incorporated into **1** during the enzymatic hydrolysis of **3**, suggestive of a mechanism involving direct hydrolytic cleavage of the ester group in **3**. Finally, 3-(ethylamino)-2-(ethylcarbamoyl)-3-oxo-2-phenylpropyl 2-(3-(dimethylcarbamoyl)-4-(4'-(trifluoromethyl)-[1,1'-biphenyl]-2-ylcarboxamido)phenyl)acetate (**4**), which possessed an *N,N*-diethyl-2-phenylmalonamide substituent (in lieu of the diethyl-2-phenylmalonate motif in JTT-130) proved to be resistant to the hydrolytic cleavage/decarboxylative fragmentation pathway that yielded **1**, a phenomenon that further confirmed our hypothesis. From a toxicological standpoint, it is noteworthy to point out that the liberation of the electrophilic acrylic acid species as a byproduct of JTT-130 hydrolysis is similar to the bioactivation mechanism established for felbamate, an anticonvulsant agent associated with idiosyncratic aplastic anemia and hepatotoxicity.



## INTRODUCTION

Microsomal triglyceride transfer protein (MTP) is an intracellular lipid-transfer protein localized in the endoplasmic reticulum of hepatocytes and enterocytes. With its broad distribution in both intestinal and hepatic tissue, MTP has been

shown to play a crucial role in the assembly of triglyceride (TG)-rich lipoproteins, such as chylomicrons in the intestine and

Received: June 2, 2012

Published: September 18, 2012

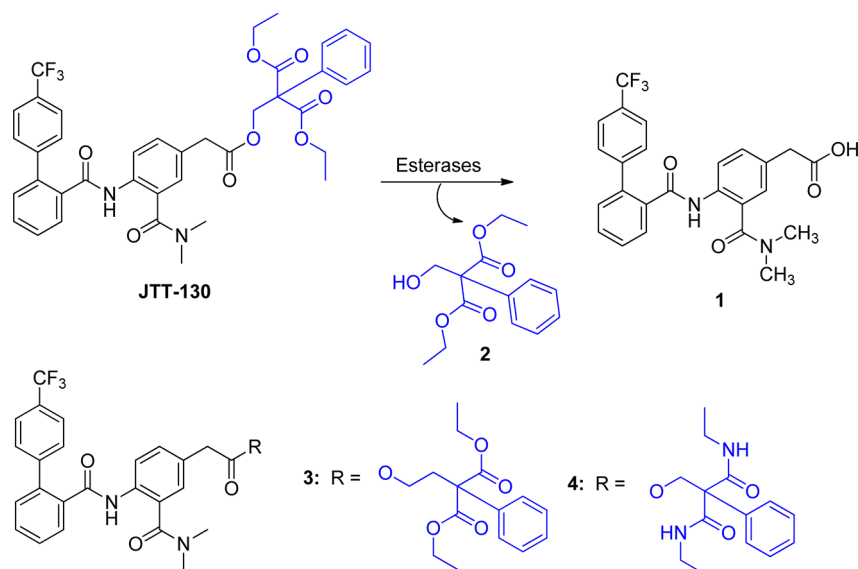


**Figure 1.** Structures of the intestine-specific MTP inhibitor JTT-130 and related ester derivatives 3 and 4.

very low density lipoprotein (VLDL) in the liver.<sup>1,2</sup> Patients with the genetic disorder abetalipoproteinemia or Bassen-Kornzweig syndrome have loss-of-function mutations in the MTP gene,<sup>3,4</sup> resulting in extremely low plasma concentrations of cholesterol and TGs and the absence of chylomicrons, VLDL and LDL-cholesterol.<sup>5</sup> The elucidation of the mechanistic basis for this disease led to the concept that small-molecule inhibitors of MTP could be beneficial in the treatment of dyslipidemia and various other metabolic disorders. Indeed, preclinical studies in animal models showed that inhibition of MTP significantly reduced serum cholesterol levels and slowed the formation of atherosclerotic plaques.<sup>6–8</sup> Furthermore, in a clinical setting, MTP inhibition was shown to significantly reduce LDL-cholesterol levels in patients with homozygous familial hypercholesterolemia.<sup>9</sup> Unfortunately, blockade of hepatic MTP is accompanied by a significant decrease in the ability of the liver to eliminate fat, and administration of systemic MTP inhibitors universally resulted in unacceptable increases in liver transaminases and increased hepatic fat deposition consistent with hepatic steatosis or “fatty liver”.<sup>8,10–13</sup> Consistent with these toxicological findings were the clinical observations associating genetic polymorphisms in the MTP gene with an increased incidence of steatosis in type II diabetic and the abetalipoproteinemic patient population.<sup>14,15</sup> Subsequently, it has been proposed that nonsystemically absorbed MTP inhibitors could alleviate the hepatotoxicity concerns by selectively inhibiting lipid transport within the enterocyte, without significantly affecting the export of hepatic TGs as VLDL, which is the underlying cause of steatosis.<sup>16–19</sup>

Diethyl 2-((2-(3-(dimethylcarbamoyl)-4-(4'-(trifluoromethyl)-[1,1'-biphenyl]-2-ylcarboxamido)phenyl)acetoxy)methyl)-2-phenylmalonate (JTT-130) has been recently described as a potent MTP inhibitor (Figure 1), which, upon oral administration to preclinical species, selectively inhibits MTP activity in the small intestine.<sup>20–23</sup> Furthermore, in contrast with non-selective MTP inhibitors, JTT-130 did not cause elevations in transaminase levels in the course of a three-month clinical trial in patients with dyslipidemia.<sup>20</sup> As such, selective inhibitory effects of JTT-130 on intestinal MTP are a function of a facile (and rapid) hydrolysis of its ester linkage by liver-specific carboxylesterase(s) to yield 2-(3-(dimethylcarbamoyl)-4-(4'-(trifluoro-

methyl)-[1,1'-biphenyl]-2-ylcarboxamido)phenyl)acetic acid (1), a pharmacologically inactive metabolite (see Figure 1).<sup>20</sup>

In conjunction with our internal tissue-specific MTP inhibitor program,<sup>8,24,25</sup> we conducted a detailed *in vitro* mechanistic assessment of the ester bond cleavage in JTT-130 using human liver microsomes. Lack of incorporation of <sup>18</sup>O in 1 that was generated upon incubating JTT-130 in human liver microsomes suggested that hydrolysis did not proceed via a simple ester bond cleavage to yield carboxylic acid 1 and the alcohol byproduct 2 as shown in Figure 1. The characterization of atropic acid (2-phenylacrylic acid) as a metabolite of JTT-130 in the microsomal incubations suggested a pathway involving the hydrolysis of one of the pendant malonate ethyl ester groups followed by decarboxylative fragmentation to 1. Additional support for our hypothesis was obtained from mechanistic studies on diethyl 2-(2-(3-(dimethylcarbamoyl)-4-(4'-(trifluoromethyl)-[1,1'-biphenyl]-2-ylcarboxamido)phenyl)acetoxy)ethyl)-2-phenylmalonate (3) and 3-(ethylamino)-2-(ethylcarbamoyl)-3-oxo-2-phenylpropyl 2-(3-(dimethylcarbamoyl)-4-(4'-(trifluoromethyl)-[1,1'-biphenyl]-2-ylcarboxamido)phenyl)acetate (4) (see Figure 1). In particular, ester 3 cannot participate in hydrolysis via the fragmentation pathway because of the presence of an additional methylene group. Unlike the case with JTT-130, <sup>18</sup>O was readily incorporated in 1 during the enzymatic hydrolysis of 3, suggestive of a mechanism involving direct hydrolytic cleavage of the ester linkage. Compound 4, which possessed an *N*<sup>1</sup>,*N*<sup>3</sup>-diethyl-2-phenylmalonamide substituent (in lieu of the diethyl-2-phenylmalonate motif in JTT-130) proved to be resistant to the hydrolytic cleavage pathway that yielded 1, a finding that provided further credence to our hypothesis. The collective findings from these studies are summarized, herein, with a particular emphasis on the JTT-130 hydrolysis mechanism that yields electrophilic  $\alpha,\beta$ -unsaturated carbonyl derivatives as byproduct.

## MATERIALS AND METHODS

**Materials.** Unless specified otherwise, starting materials used in the chemical synthesis are available from commercial sources such as Sigma Aldrich (Milwaukee, WI), Lancaster Synthesis, Inc. (Windham, NH), Acros Organics (Fairlawn, NJ), Maybridge Chemical Company, Ltd. (Cornwall, England), Mallinckrodt Baker (Phillipsburg NJ), and EMD (Gibbstown, NJ). Atropic acid was obtained from Apollo Scientific Ltd.

(Cheshire, England). Solvents used for analysis were of analytical or HPLC grade (Fisher Scientific, Pittsburgh, PA, USA). Dimethyl sulfoxide (DMSO)- $d_6$  "100%" was purchased from Cambridge Isotope Laboratories (Andover, MA, USA). Chemical shifts are expressed in parts per million (ppm) relative to the residual solvent as an internal reference. The peak shapes are denoted as follows: s, singlet; d, doublet; dd, doublet of doublets; t, triplet; td, triplet of doublets; q, quartet; m, multiplet and brs, broad singlet. Coupling constants ( $J$ ) are given in hertz (Hz). Glutathione (GSH) and NADPH were obtained from Sigma Aldrich (St. Louis, MO). Human liver microsomal fractions pooled from 53 individual donors were purchased from BD Gentest (Woburn, MA).

JTT-130, **1**, **3**, and **4** were synthesized using the general methods described in the Japan Tobacco patent.<sup>26</sup> JTT-130:  $^1\text{H}$  NMR (400 MHz,  $\text{CDCl}_3$ )  $\delta$  1.22 (t,  $J$  = 7.1 Hz, 6 H), 2.81 (brs, 3 H), 2.94 (brs, 3 H), 3.52 (s, 2 H), 4.22 (q,  $J$  = 7.1 Hz, 4 H), 4.83 (s, 2 H), 7.04 (d,  $J$  = 1.9 Hz, 1 H), 7.21 (dd,  $J$  = 8.7, 2.2 Hz, 1 H), 7.28–7.34 (m, 5 H), 7.40 (dd,  $J$  = 7.5, 1.1 Hz, 1 H), 7.47–7.57 (m,  $J$  = 14.7, 6.7, 6.7, 6.6 Hz, 2 H), 7.62 (s, 4 H), 7.70 (dd,  $J$  = 7.4, 1.2 Hz, 1 H), 8.36 (d,  $J$  = 8.5 Hz, 1 H), 9.18 (s, 1 H). Liquid chromatography–mass spectrometry (electrospray ionization (ESI)):  $\text{MH}^+$  = 719.3 (100%).

**Compound 1.**  $^1\text{H}$  NMR (400 MHz,  $\text{CDCl}_3$ )  $\delta$  2.84 (brs, 3 H), 2.96 (brs, 3 H), 3.54 (s, 2 H), 7.09 (d,  $J$  = 2.0 Hz, 1 H), 7.24–7.28 (m, 1 H), 7.39 (d,  $J$  = 7.5 Hz, 1 H), 7.45–7.56 (m, 2 H), 7.59–7.64 (m, 4 H), 7.68 (dd,  $J$  = 7.5, 1.0 Hz, 1 H), 8.25 (d,  $J$  = 8.5 Hz, 1 H), 9.08 (s, 1 H). Liquid chromatography–mass spectrometry (ESI)  $\text{MH}^+$  = 471.4 (100%).

**Compound 3.**  $^1\text{H}$  NMR (400 MHz,  $\text{CDCl}_3$ )  $\delta$  1.25 (t,  $J$  = 7.1 Hz, 6 H), 2.62 (t,  $J$  = 7.2 Hz, 2 H), 2.86 (brs, 3 H), 2.95 (brs, 3 H), 3.47 (s, 2 H), 4.08 (t,  $J$  = 7.2 Hz, 2 H), 4.18–4.30 (m, 4 H), 7.09 (d,  $J$  = 2.1 Hz, 1 H), 7.25 (dd,  $J$  = 8.5, 2.0 Hz, 1 H), 7.28–7.41 (m, 6 H), 7.49 (td,  $J$  = 7.4, 1.5 Hz, 1 H), 7.54 (td,  $J$  = 7.5, 1.6 Hz, 1 H), 7.59–7.64 (m, 4 H), 7.70 (dd,  $J$  = 7.5, 1.3 Hz, 1 H), 8.36 (d,  $J$  = 8.5 Hz, 1 H), 9.15 (s, 1 H). Liquid chromatography–mass spectrometry (ESI)  $\text{MH}^+$  = 733.4 (100%).

**Compound 4.**  $^1\text{H}$  NMR (500 MHz,  $\text{CDCl}_3$ )  $\delta$  1.08 (t,  $J$  = 7.32 Hz, 6 H), 2.85 (brs, 3 H), 2.96 (brs, 3 H), 3.20–3.31 (m, 4 H), 3.55 (s, 2 H), 4.84 (s, 2 H), 7.04 (d,  $J$  = 1.71 Hz, 1 H), 7.12 (t,  $J$  = 4.90 Hz, 2 H), 7.16–7.24 (m, 3 H), 7.29–7.35 (m, 3 H), 7.41 (d,  $J$  = 7.32 Hz, 1 H), 7.50 (td,  $J$  = 7.60, 1.20 Hz, 1 H), 7.55 (td,  $J$  = 7.60, 1.22 Hz, 1 H), 7.58–7.65 (m, 4 H), 7.70 (d,  $J$  = 6.83 Hz, 1 H), 8.39 (d,  $J$  = 8.54 Hz, 1 H), 9.19 (s, 1 H). Liquid chromatography–mass spectrometry (ESI)  $\text{MH}^+$  = 717.5 (100%).

**Hydrolytic Stability in Human Liver Microsomes.** Stock solutions of test compounds were prepared in acetonitrile. Compounds (final concentration = 1  $\mu\text{M}$ ) were incubated with human liver microsomes (cytochrome P450 (P450) concentration = 0.27  $\mu\text{M}$  and protein concentration = 0.76 mg/mL) in 0.05 M potassium phosphate buffer (pH 7.4) at 37 °C in a shaking water bath. The total incubation volume was 0.5 mL. Aliquots (25  $\mu\text{L}$ ) of the reaction mixture at 0, 2, 4, 6, 8, 10, 20, and 30 min (time period associated with reaction linearity) were added to acetonitrile (200  $\mu\text{L}$ ) containing a proprietary internal standard (MW = 704, 0.1  $\mu\text{g/mL}$ ) and were analyzed for disappearance of the substrate by liquid chromatography tandem mass spectrometry (LC-MS/MS). Analyte concentrations were monitored on a Sciex API 3000 LC-MS/MS triple-quadrupole mass spectrometer. Analytes were chromatographically separated using a Shimadzu LC-20 AD HPLC system. An autosampler was programmed to inject 20  $\mu\text{L}$  on a Synergi Polar RP 2  $\mu\text{m}$ , 30  $\times$  2.0 mm column using a mobile phase consisting of 95:5 water/acetonitrile containing 0.1% formic acid (solvent A) and 95:5 acetonitrile/water (solvent B). The LC conditions were programmed as follows: 10% acetonitrile for 0.5 min, increasing to 90% over the next 1.8 min and then decreasing back to 10% (i.e., the original condition) over the final 3 min, at a flow rate of 0.5 mL/min. Ionization was conducted in the positive ion mode at an ion-spray interface temperature of 400 °C, using nitrogen as the nebulizing and heating gas. The ion-spray voltage was 5.0 kV, and the orifice voltage was optimized at 30 eV. JTT-130, **3** and **4**, and the internal standard were analyzed in the multiple-reaction monitoring mode using the transitions  $[\text{MH}]^+$  to product ion  $m/z$  +  $\text{H}^+$  719  $\rightarrow$  674, 733  $\rightarrow$  688, and 717  $\rightarrow$  672, respectively. For half-life ( $t_{1/2}$ ) determinations for substrate depletion in microsomes, substrate/internal standard peak height ratios were determined and normalized to the value obtained at time  $t$  = 0. The

percentage of substrate remaining versus time was fitted to first-order decay functions to yield *in vitro*  $t_{1/2}$  values. If the test substrate demonstrated nonlinearity on log percentage remaining versus time curves, only those initial time points wherein log-linearity was observed were used to determine  $t_{1/2}$  values.  $t_{1/2}$  values reported are the mean of two independent experiments.

#### Metabolite Identification in Human Liver Microsomes.

Incubations were carried out at 37 °C for 0 and 30 min in a shaking water bath. The incubation volume was 1 mL and consisted of microsomes (protein concentration = 1.0 mg/mL) and test compounds (10  $\mu\text{M}$ ) in 0.1 M potassium phosphate buffer (pH 7.4) and  $\text{MgCl}_2$  (3.3 mM). The formation of GSH conjugates of reactive species derived from JTT-130 metabolism was examined via the inclusion of 1 mM GSH in the human liver microsomal incubations. Reactions were terminated by the addition of ice-cold acetonitrile (3 mL). The solutions were centrifuged (3000g, 15 min), and the supernatants were transferred to clean 15 mL glass centrifuge tubes and concentrated to dryness. The residue was reconstituted with 200  $\mu\text{L}$  of mobile phase and analyzed for metabolite formation using LC-MS/MS.

**$^{18}\text{O}$  Incorporation Studies.** The source of oxygen incorporated in the carboxylic acid metabolite **1** was characterized using 97%  $\text{H}_2^{18}\text{O}$  (Cambridge Isotope Laboratories Inc., Andover, MA). For  $\text{H}_2^{18}\text{O}$  studies, 15 mL glass centrifuge tubes containing 1.0 mL of 100 mM potassium phosphate (pH 7.4) were concentrated to dryness using an evaporative centrifuge.  $\text{H}_2^{18}\text{O}$  (0.925 mL) was added to the dried centrifuge tube containing phosphate buffer. Potassium phosphate (pH 7.4) buffered  $\text{H}_2^{18}\text{O}$  was used to create 1.0 mL incubations containing test compounds JTT-130 and **3** (at a concentration of 10  $\mu\text{M}$ ), and 3.3 mM  $\text{MgCl}_2$  (20  $\mu\text{L}$ ), in human liver microsomes (protein concentration = 1.0 mg/mL). The isotopic enrichment of  $\text{H}_2^{18}\text{O}$  was ~89.7%. The sample was placed in a shaking water bath set to 37 °C. After 30 min, the reactions were quenched with 3.0 mL of acetonitrile and centrifuged at 3000g for 5 min. The supernatant was transferred to a clean 15 mL centrifuge tube and concentrated to dryness. The samples were analyzed for  $^{18}\text{O}$  incorporation by LC-MS/MS.

#### LC-MS/MS Methodology for Metabolite Identification Studies.

The HPLC system consisted of an Acella quaternary solvent delivery pump, an Acella autoinjector, and a Surveyor PDA Plus photodiode array detector (Thermo Electron Corporation, Waltham, MA). Chromatography was performed on a Phenomenex Hydro RP column (4.6 mm  $\times$  150 mm, 4  $\mu\text{m}$ ). The mobile phase was composed of 5 mM ammonium formate buffer (pH 3.0) (solvent A) and acetonitrile (solvent B). The flow rate was 1.0 mL/min. The LC gradient started at 15% B for 5 min, was ramped linearly to 90% B over 35 min, held at 90% B over 10 min, returned to the initial condition over 1.0 min, and allowed to equilibrate for 4.0 min. Postcolumn flow passed through the PDA detector to provide UV ( $\lambda$  = 254 nm) detection prior to being split to the mass spectrometer such that the mobile phase was introduced into the electrospray source at a rate of 100  $\mu\text{L/min}$ . The LC system was interfaced to a Thermo Orbitrap mass spectrometer operating in positive ion electrospray mode. Xcalibur software, version 2.0, was used to control the HPLC/MS system. Full scan data were collected at 15,000 resolution. Data dependent product ion scans of the two most intense ions found in the full scan were obtained at 15,000 resolution. The dynamic exclusion function was used with a 1 min exclusion duration after 3 successive product ion scans with an early exclusion if the precursor ion falls below a signal-to-noise of 20. Additional data dependent scanning was performed on select samples at unit mass resolution for product ions of the two most intense ions found in the full scan mode.

**Biosynthesis and NMR Analysis of the " $m/z$  363" Metabolite M2 Obtained from the Enzyme-Catalyzed Hydrolysis of JTT-130.** Metabolite M2 detected in the course of JTT-130 hydrolysis was biosynthesized via a scale-up of the human microsomal incubations (protein concentration = 10 mg/mL, 1 h at 37 °C) of JTT-130 (100  $\mu\text{M}$ ) in a total of four 50 mL polypropylene centrifuge tubes (10 mL incubation/tube). Cold acetonitrile (20 mL) was added to each tube, and samples were centrifuged at 3000g for 15 min. The supernatants were transferred to clean 50 mL polypropylene centrifuge tubes and concentrated to dryness. The residue in each tube was reconstituted in

250  $\mu\text{L}$  of 10% acetonitrile in water. Reconstituted residues were combined in a 2 mL HPLC vial and were injected onto an HPLC

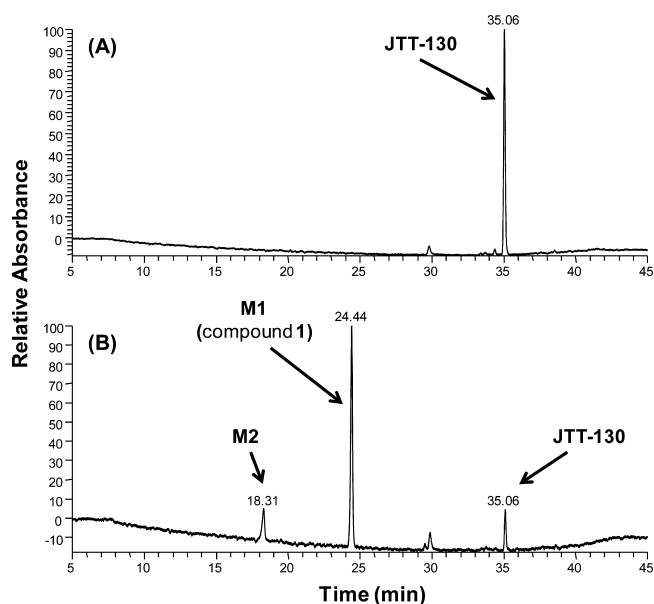


**Figure 2.** LC-UV ( $\lambda = 254$  nm) chromatograms of incubations of JTT-130 (10  $\mu\text{M}$ ) in human liver microsomes (in the absence of NADPH) at  $t = 0$  min (panel A) and at  $t = 30$  min (panel B). Incubations were conducted at  $37^\circ\text{C}$  in a shaking water bath.

semipreparative system using three injection volumes of approximately 330  $\mu\text{L}$ . The semipreparative system consisted of a Shimadzu SiL-HTC autosampler, two LC-20AD solvent pumps, an SPD-M20A diode array detector, and a FRC-10A fraction collector. Separation was performed on a Zorbax RX C8,  $9.4 \times 250$  mm, 5  $\mu\text{M}$  semipreparative HPLC column. The mobile phase was composed of 5 mM ammonium formate buffer (pH 3.0) (solvent A) and acetonitrile (solvent B). The flow rate was 4.0 mL/min. The LC gradient started at 15% B for 5 min, was ramped linearly to 90% B over 35 min, held at 90% B over 10 min, returned to the initial condition over 1.0 min, and allowed to equilibrate for 4.0 min. HPLC fractions were collected throughout the run at 1 min intervals into glass culture tubes. Aliquots (100  $\mu\text{L}$ ) of fractions at the retention time ( $t_R$ ) of the UV peak believed to be the unknown metabolite M2 (tentatively assigned as  $\text{MH}^+ = 363$ ) were analyzed by LC/MS for verification. Fractions containing the peak ( $\text{MH}^+ = 363$ ) were combined into a single 15 mL glass centrifuge tube and concentrated to dryness. The residue was then evacuated in a drybox for about two hours prior to being reconstituted in  $\text{DMSO}-d_6$  for NMR studies. NMR spectra were recorded on a Bruker Avance 600 MHz instrument (Bruker BioSpin Corporation, Billerica, MA) controlled by TOPSPIN V2.1 and equipped with a 5 mm cryo-TCI probe. Synthetic samples and isolated materials were dissolved in 0.15 mL of  $\text{DMSO}-d_6$ . All spectra were referenced using residual  $\text{DMSO}-d_6$  ( $\delta = 2.5$  ppm relative to TMS,  $\delta = 0.00$ ). 1D spectra were recorded using a sweep width of 8000 Hz and a total recycle time of 3.6 s. The resulting time-averaged free induction decays were transformed using an exponential line broadening of 1.0 Hz to enhance signal-to-noise. Multiplicity edited heteronuclear single quantum coherence (HSQC) and heteronuclear multiple bond correlation (HMBC) data were recorded using the standard pulse sequences provided by Bruker. 2D NMR data were

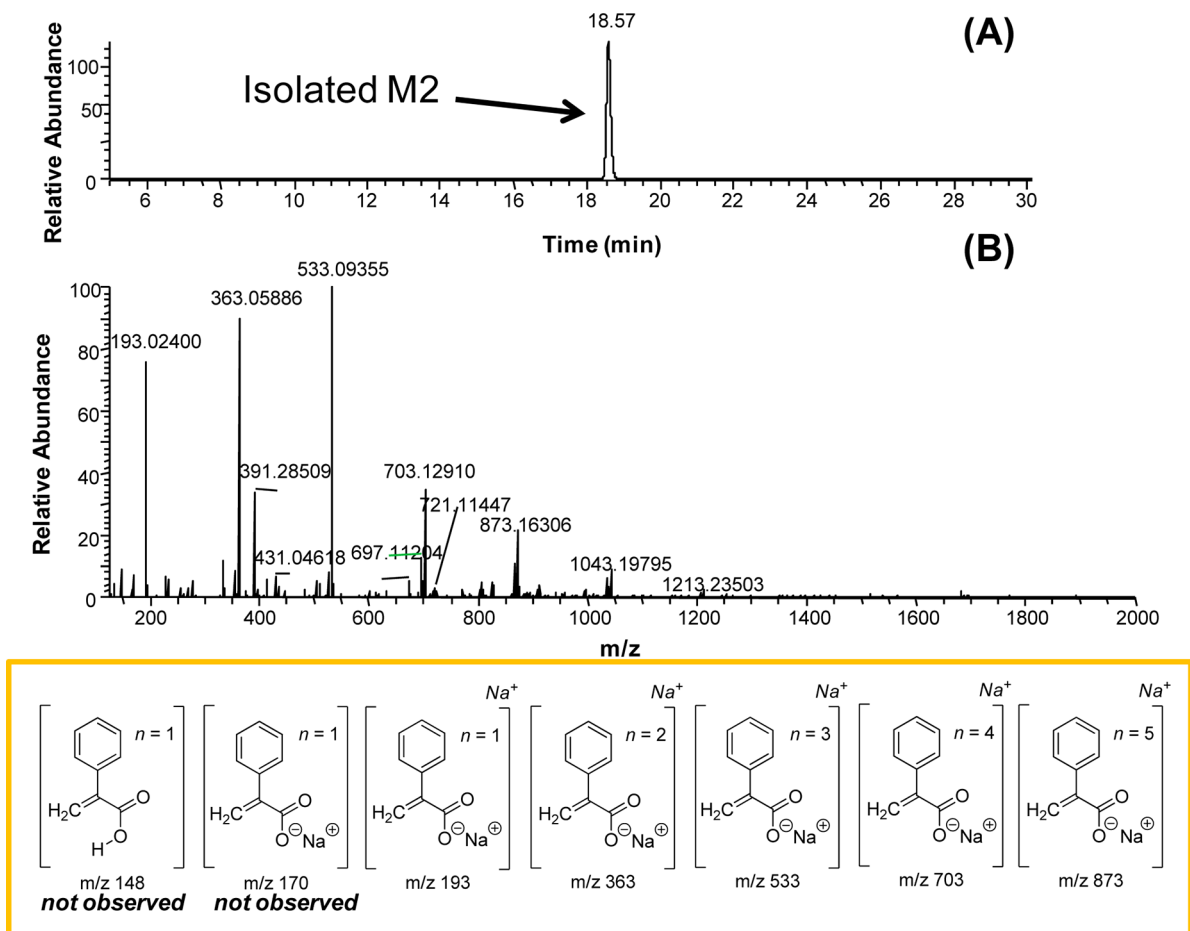


**Figure 3.** LC-UV ( $\lambda = 254$  nm) chromatogram (panel A) and mass spectrum (panel B) of isolated M2 ( $t_R = 18.31$  min). Structures depict the fragment ions discerned in the mass spectrum of M2.



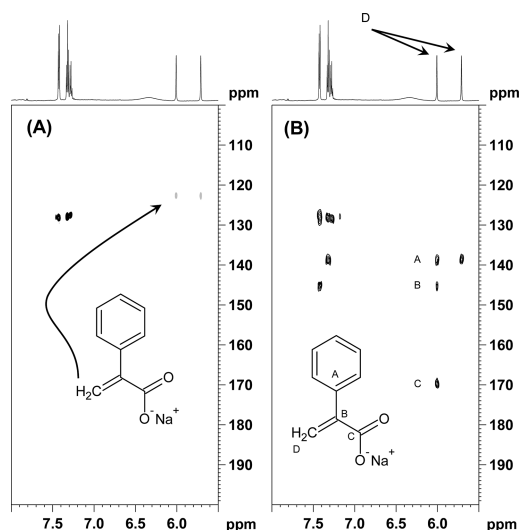


**Figure 4.** Expanded aromatic region of the  $^1\text{H}$ - $^{13}\text{C}$  multiplicity edited HSQC (panel A) and HMBC (panel B) spectra of M2.

typically acquired using a  $1\text{K} \times 128$  data matrix with 16 dummy scans. The data was zero-filled to a size of  $1\text{K} \times 1\text{K}$ . Unless otherwise noted, for 2D NMR experiments, a relaxation delay of 1.5 s was used between transients.

## RESULTS

**Stability of JTT-130, 3, and 4 in Human Liver Microsomes.** To examine microsomal stability, test compounds (JTT-130, 3, and 4) at a concentration of  $1\text{ }\mu\text{M}$  were incubated in human liver microsomes at  $37\text{ }^\circ\text{C}$  in the presence or absence of NADPH cofactor; periodically, aliquots of the incubation mixture were examined for substrate depletion. The  $t_{1/2}$  for depletion of JTT-130, 3, and 4 in human liver microsomes in the absence of NADPH were 1.2 min, 1.4 min, and  $>60$  min, respectively. The  $t_{1/2}$  for the depletion of JTT-130, 3, and 4 in human liver microsomes in the presence of NADPH were 1.3, 1.4, and 2.4 min, respectively. The rapid degradation of JTT-130 in human liver microsomes ( $\pm$ NADPH) appears to be in general agreement with the previous results of Mera et al.,<sup>20</sup> wherein,  $\sim 85\%$  of JTT-130 was consumed in a 5 min incubation with the human liver S9 fraction.

**Metabolite Identification in Human Liver Microsomes.**  
**Metabolism of JTT-130.** LC-UV/MS traces of human liver microsomal incubations of JTT-130 ( $10\text{ }\mu\text{M}$ ), conducted at  $37\text{ }^\circ\text{C}$  for 30 min are shown in Figure 2. Examination of the metabolic profile of human liver microsomal incubations of JTT-130 in the absence of NADPH revealed near complete conversion of the parent compound and the appearance of two metabolites (designated as M1 and M2). A similar metabolic profile was discerned in JTT-130 incubations in liver microsomes in the presence of NADPH (data not shown). The  $t_R$  (24.44 min) and collision-induced dissociation (CID) spectrum for metabolite M1 ( $\text{MH}^+$  at  $m/z$  471.1526  $\rightarrow$  426.0947 (100%), loss of dimethylamine) were identical to those discerned with an authentic standard of the carboxylic acid **1** (Figure 1S, Supporting Information). Metabolite M2 ( $t_R = 18.31$  min) displayed a  $\text{MH}^+$  at  $m/z$  363.05886, which does not correspond with the protonated molecular mass of the primary alcohol metabolite **2** that can be obtained via the JTT-130 hydrolysis route depicted in Figure 1 or with possible downstream ester hydrolysis products of **2**, namely, 3-ethoxy-2-(hydroxymethyl)-3-oxo-2-phenylpropanoic acid ( $\text{MH}^+ = 239.0914$ ) and

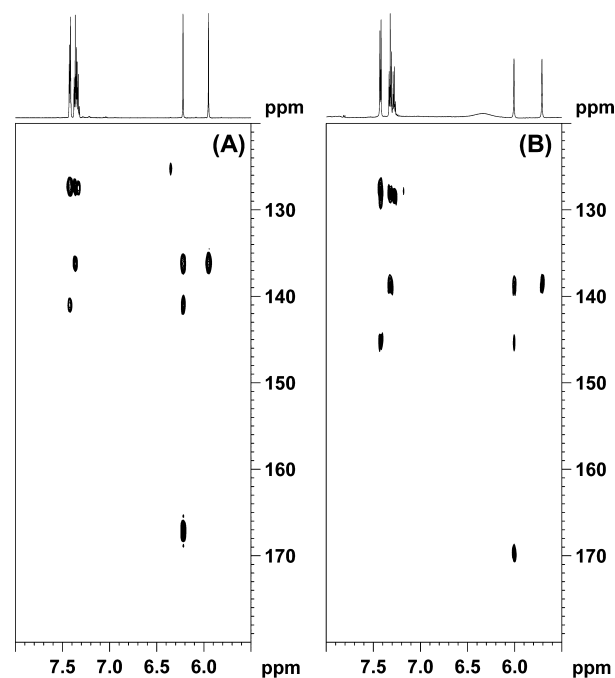


**Figure 5.** Comparison of the HMBC NMR spectra of an authentic standard of atropic acid (panel A) and isolated M2 (panel B).

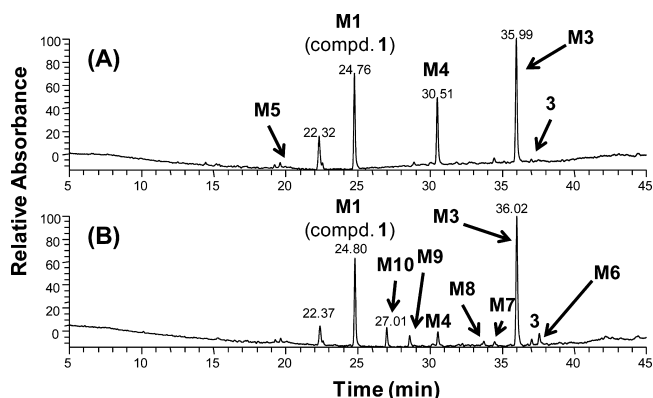


**Figure 6.** LC-UV ( $\lambda = 254\text{ nm}$ ) chromatograms of incubations of **3** ( $10\text{ }\mu\text{M}$ ) in human liver microsomes at  $t = 30$  min in the absence of NADPH (panel A) and  $t = 30$  min in the presence of NADPH (panel B). Incubations were conducted at  $37\text{ }^\circ\text{C}$  in a shaking water bath. The peak at  $t_R = 22.30$  min is background noise.

2-(hydroxymethyl)-2-phenylmalonic acid ( $\text{MH}^+ = 211.0601$ ). Furthermore, attempts to generate a CID spectrum of M2 were unsuccessful, raising the question of whether  $m/z$  363 was the actual protonated molecular mass of the metabolite.

**Isolation and Structural Characterization of M2.** Unknown metabolite M2 was isolated by semipreparative HPLC fraction collection of human liver microsomal incubations of JTT-130. MS data of the M2 isolate was complex with no clear single  $\text{MH}^+$  ion (Figure 3). The spectra contained repeating ions differing by  $170.0348\text{ Da}$  starting at  $m/z$  193.0236 with the last observable ion at  $m/z$  1213.2350. Exact mass data suggested that M2 ( $m/z = 363.05886$ ) could be the product of 2-phenylacrylic acid (i.e., atropic acid) with  $m/z$  193 being the dissociated singly charged species and the  $170\text{ amu}$  intervals being the neutral addition of subsequent sodium 2-phenylacrylate molecules (Figure 3).  $^1\text{H}$  NMR analysis of this material indicated that the isolate contained five aromatic resonances, two olefinic

resonances, and a complete absence of aliphatic resonances. Multiplicity edited HSQC and HMBC NMR spectra positively identified two olefinic protons proximal to the carbonyl carbon

and an aromatic ring, which is consistent with the structure of atropic acid (Figure 4). Unambiguous confirmation of the structure was obtained via comparison of the NMR characteristics of

Table 1. LC-MS/MS Data for 3 and Its Metabolites in Human Liver Microsomes

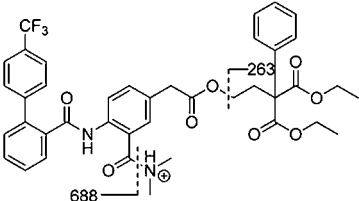
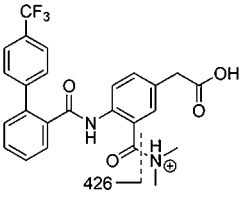
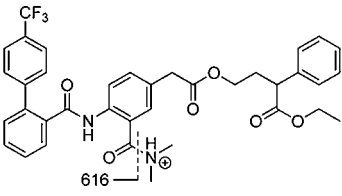
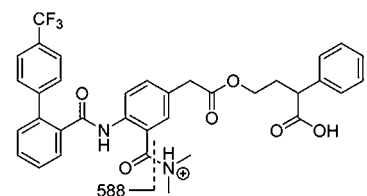
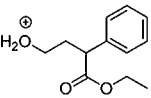
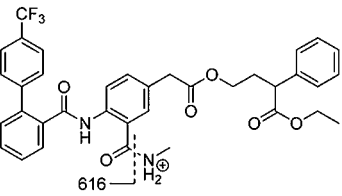
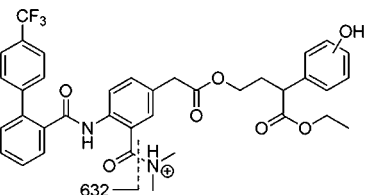
Compound	Co-factor <sup>a</sup>	t <sub>r</sub> (min) <sup>b</sup>	Observed MH <sup>+</sup>	LC-MS <sup>n</sup> fragments, m/z	Structure
3	N.A.	37.0	733.2731	688.2141, 263.1277	
M1/1	± NADPH	24.44	471.1526	426.0947	
M3	± NADPH	35.9	661.2521	616.1945	
M4	± NADPH	30.5	633.2207	588.1632	
M5	± NADPH	17.7	209.1172	N.D.	
M6	+ NADPH	37.5	647.2363	616.1946	
M7	+ NADPH	34.5	677.2469	632.1895	

Table 1. continued

Compound	Co-factor <sup>a</sup>	<i>t<sub>r</sub></i> (min) <sup>b</sup>	Observed MH <sup>+</sup>	LC-MS <sup>n</sup> fragments, <i>m/z</i>	Structure
M8	+ NADPH	33.8	677.2469	632.1898, 614.1792, 426.0949	<p><math>m/z\ 677 \xrightarrow{-H_2O, -HN(CH_3)_2} m/z\ 614</math></p>
M9	+ NADPH	28.5	649.2156	604.1582, 586.1474, 426.0950	<p><math>m/z\ 649 \xrightarrow{-H_2O, -HN(CH_3)_2} m/z\ 586</math></p>
M10	+ NADPH	26.9	457.1369	426.0945	

<sup>a</sup>Human liver microsomal incubations with **2** in the presence or absence of NADPH cofactor. <sup>b</sup>Under the HPLC conditions noted in Materials and Methods.

isolated M2 with the commercially available atropic acid standard (Figure 5, panels A and B). The finding that atropic acid formed ion clusters under the electrospray ionization conditions was not altogether surprising. Ion cluster formation is common in soft ionization techniques such as electrospray ionization and has been noted with carboxylic acid derivatives under similar conditions.<sup>28</sup>

**Metabolism of 3.** LC-UV/MS traces of human liver microsomal incubations of **3** (10  $\mu$ M), conducted at 37 °C for 30 min, are shown in Figure 6. Table 1 reveals the molecular weights, *t<sub>R</sub>*, CID spectral data, and proposed assignments for **3** and its metabolites. In the absence of the NADPH cofactor, the metabolic profile revealed complete consumption of the parent ester **3** (MH<sup>+</sup> = 733.2731, *t<sub>R</sub>* = 37.0 min), and the concomitant formation of four metabolites, carboxylic acid **1** and M3–M5 (Figure 6, Panel A). M3 (*t<sub>R</sub>* = 35.99 min) displayed a MH<sup>+</sup> at *m/z* 661.2521, which corresponds to a loss of one of the pendant ethyl ester moieties (−72.021 Da) in **3**. The CID spectrum of M3 displayed a diagnostic fragment ion at *m/z* 616.1945 corresponding to the loss of the *N,N*-dimethylamine motif, which supported the proposed structural assignment for M3, shown in Table 1. Metabolite M4 (*t<sub>R</sub>* = 30.5 min) displayed a MH<sup>+</sup> at *m/z* 633.2207, which corresponds to a loss of the ethyl group (−28.0314 Da) from metabolite M3. The CID spectrum of M4 displayed a characteristic fragment ion at *m/z* 588.1632 corresponding to the loss of the *N,N*-dimethylamine motif, which supported the proposed structural assignment for M4, shown in Table 1. The mass spectral data (MH<sup>+</sup> at *m/z* 471.1526 → 426.0947 loss of dimethylamine) for the metabolite, which

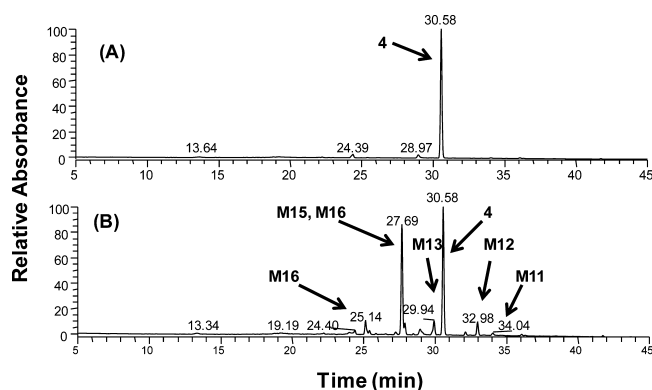


**Figure 7.** LC-UV ( $\lambda$  = 254 nm) chromatograms of incubations of **4** (10  $\mu$ M) in human liver microsomes at *t* = 30 min in the absence of NADPH (panel A) and *t* = 30 min in the presence of NADPH (panel B). Incubations were conducted at 37 °C in a shaking water bath.

eluted at *t<sub>R</sub>* = 24.7 min was identical to the one discerned for M1 (i.e., the carboxylic acid derivative **1**). Finally, the structure of metabolite M5 (*t<sub>R</sub>* = 17.7 min), which displayed a MH<sup>+</sup> at *m/z* 209.1172, was consistent with ethyl 4-hydroxy-2-phenylbutanoate, the alcohol obtained upon direct hydrolysis of the ester linkage in M3.

In the presence of the NADPH cofactor, LC-UV/MS analysis also revealed near complete consumption of ester **3** and formation of carboxylic acid **1**, M3, and M4. Trace levels of downstream oxidative metabolites of **1**, M3, and M4, i.e.,

M6–M10, were also detected in the presence of the NADPH cofactor (Figure 6, panel B). Metabolites M6 ( $t_R = 37.5$  min) and M10 ( $t_R = 26.9$  min) displayed protonated molecular ions at  $m/z$  647.2363 and 457.1369, which corresponded to the loss of 14.015 Da from the molecular masses of M3 and **1**, respectively. The presence of diagnostic fragment ions at  $m/z$  616.1946 and 426.0945 in the CID spectra of M6 and M10 established that they were N-demethylated metabolites of M3 and **1**, respectively. Metabolites M7 ( $t_R = 34.5$  min) and M8

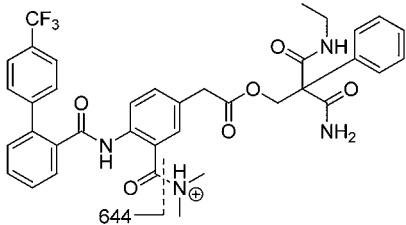
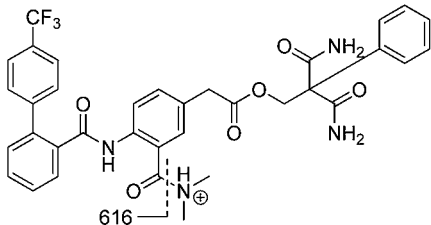
( $t_R = 33.8$  min) indicated protonated molecular masses at  $m/z$  677.2469 implying that they were isomers derived from the monohydroxylations of M3. Both metabolites possessed a common fragment ion at  $m/z \sim 632.189$ , which ruled out the *N,N*-dimethylamine motif as the site(s) of hydroxylation. The presence of a fragment ion at  $m/z$  614.1792 in the CID spectrum of M8 was consistent with a loss of a water molecule, suggesting that the site of oxidation was on an aliphatic hydrogen (i.e., on one of the two methylene or methine hydrogens) in the alcohol

**Table 2.** LC-MS/MS Data for **4** and Its Metabolites in Human Liver Microsomes

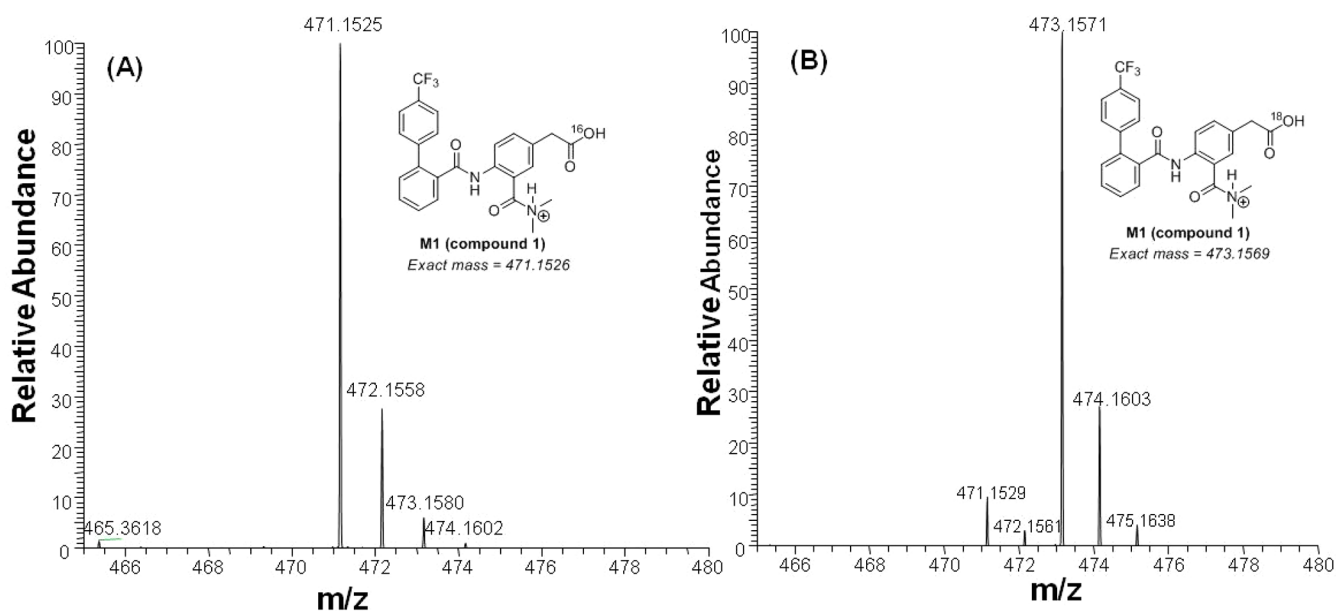
Compound	$t_R$ (min) <sup>a</sup>	Observed $MH^+$	LC-MS <sup>n</sup> fragments, $m/z$	Structure
<b>4</b>	30.6	717.2894	672.2315, 644.2004	
M11	34.1	701.2581	670.2159, 644.2005	
M12	33.0	703.2738	672.2315	
M13	29.9	675.2425	644.2004	
M14	27.7	715.2738	670.2157	



Table 2. continued

Compound	$t_r$ (min) <sup>a</sup>	Observed $MH^+$	LC-MS $n$ fragments, $m/z$	Structure
M15	27.6	689.2581	644.2004	
M16	25.1	661.2268	616.1690	

<sup>a</sup>Under the HPLC conditions noted in Materials and Methods.



**Figure 8.** Examination of  $^{18}O$  incorporation in the carboxylic acid metabolite **1** obtained from the hydrolysis of JTT-130 (panel A) and **3** (panel B) in human liver microsomes in the presence of  $H_2^{18}O$ .

substituent of M3. We speculate that the site of oxidation in M8 is on the methine hydrogen based on the proposed mechanism leading to the fragment ion  $m/z$  426.0949 (see Table 1). The absence of  $m/z$  614 and  $m/z$  426 fragment ions in the CID spectrum of M7 suggested that M7 was derived from an aromatic hydroxylation on the alcohol unit in M3. Metabolite M9 ( $t_R = 28.5$  min) was a monohydroxylated metabolite of M4 with a  $MH^+$  at  $m/z$  649.2156 (15.9949 Da higher than the  $MH^+$  observed for M4) and fragment ions at  $m/z$  604.1582, 586.1474, and 426.0950. The fragment ions at  $m/z$  604.1582 and 426.0950 ruled out hydroxylation on the substituent attached to the carboxylic acid portion in M4, whereas the ion at  $m/z$  586.1474 derived from the loss of a water molecule suggested that the site of oxidation was on an aliphatic hydrogen (i.e., on one of the two

methylene or methine hydrogens) in the alcohol substituent in M4. Similar to the situation with M8, we propose the methine hydrogen as the likely site for P450 oxidation in M9 based on the proposed mechanism leading to the fragment ion at  $m/z$  426.0950 (Table 1).

**Metabolism of 4.** LC-UV/MS traces of human liver microsomal incubations of **4** (10  $\mu M$ ), conducted at 37 °C for 30 min, are shown in Figure 7. Table 2 reveals the molecular weights,  $t_R$ , CID spectral data, and proposed structural assignments for **4** and its metabolites. In the absence of the NADPH cofactor, **4** was resistant to metabolic turnover in human liver microsomes (Figure 7, panel A). In the presence of the NADPH cofactor, the metabolic profile revealed the formation of six metabolites M11–M16 (alongside the parent compound **4**)

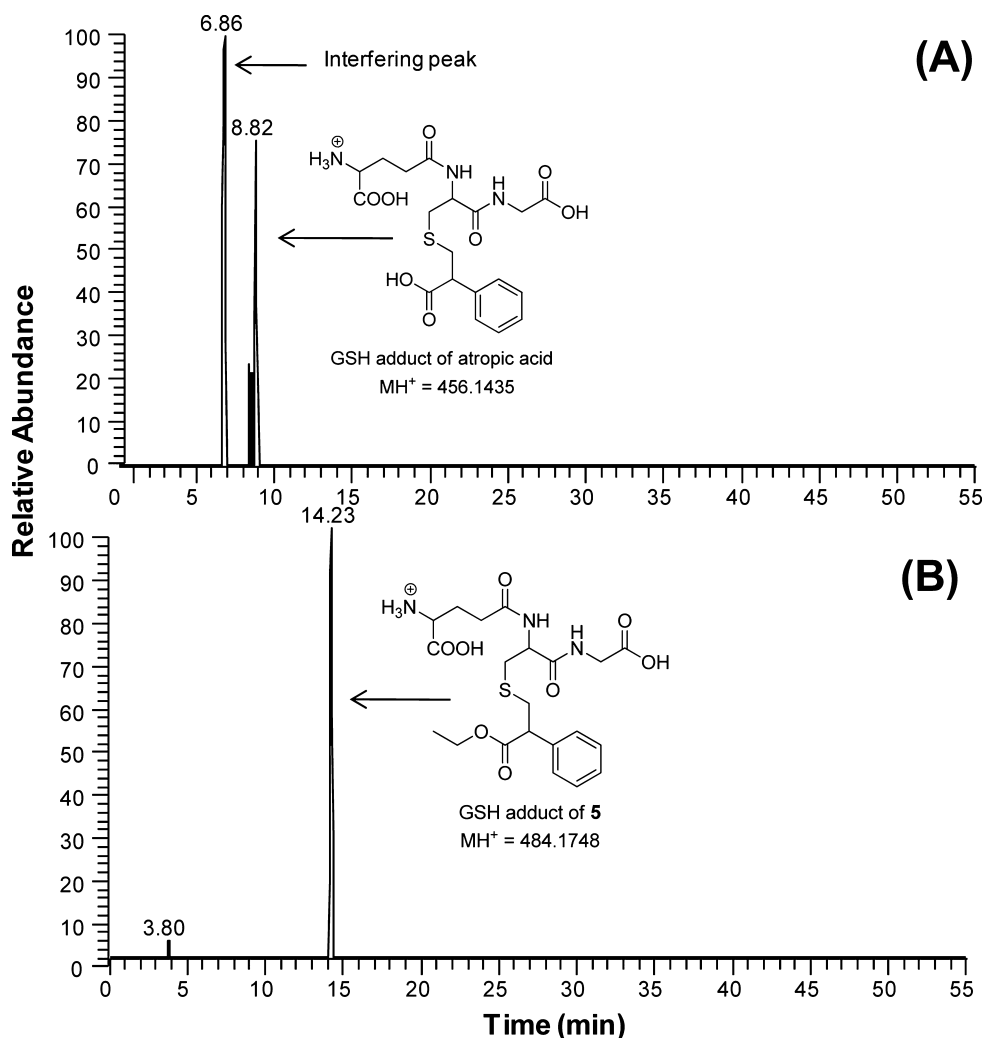


**Figure 9.** Extracted ion chromatogram of the glutathione conjugates of atropic acid (panel A) and its ethyl ester (panel B) obtained upon incubating JTT-130 in human liver microsomes in the presence of GSH.

(Figure 7, panel B). M11 ( $t_R = 34.1$  min) revealed a MH<sup>+</sup> at  $m/z$  701.2581, which is 16.0313 Da lower than the MH<sup>+</sup> of 717.2894 for the parent compound **4**. The fragment ion at  $m/z$  670.2159 in the CID spectrum of M11 is 2.0156 Da lower than the corresponding fragment ion ( $m/z = 672.2315$ ) in the mass spectrum of **4**, implying that M11 is derived from an (a) N-demethylation of the *N,N*-dimethylcarboxamide motif and (b) desaturation of one of the pendant *N*-ethylamide substituents. M12 ( $t_R = 33.0$  min) revealed a MH<sup>+</sup> at  $m/z$  703.2738, which was 14.0156 Da lower than the MH<sup>+</sup> of 717.2894 for the parent compound **4**. Furthermore, M12 displayed a fragment ion at  $m/z$  672.2315 that is identical to the one observed for **4**. This finding suggests that M12 is derived from an N-demethylation of the *N,N*-dimethylcarboxamide motif in **4**.

In the case of M13 ( $t_R = 29.9$  min), the protonated molecular and fragment ions at  $m/z$  675.2425 and  $m/z$  644.2004 were 28.031 Da lower than the corresponding values noted with M12, indicating that M13 is obtained from the N-deethylation of one of the pendant *N*-ethylamide groups in M12. The protonated molecular and fragment ions at  $m/z$  715.2738 and 670.2157 for metabolite M14 ( $t_R = 27.7$  min) were consistent with oxidative desaturation on one of the pendant ethyl amide substituents in **4** to yield the corresponding enamide metabolite. Metabolites M15 ( $t_R = 27.6$  min) and M16 ( $t_R = 25.1$  min) displayed protonated

molecular ions at  $m/z$  689.2581 and 661.2268, which corresponded to the loss of 28.0313 and 56.0626 Da, respectively, from the MH<sup>+</sup> of 717.2894 for the parent compound **4**. The presence of fragment ions at  $m/z$  644.2004 and 616.1690 in the CID spectra of M15 and M16 suggested that these metabolites were derived from sequential N-deethylation of the two pendant amide groups in **4**. Importantly, the carboxylic acid metabolite **1** was not detected as a metabolite of **4** in the human liver microsomal incubations.

**<sup>18</sup>O Incorporation Studies.** Feasibility of direct ester hydrolysis in JTT-130 via the pathway depicted in Figure 1 was probed by using H<sub>2</sub><sup>18</sup>O in microsomal incubations. LC-UV/MS analysis of a human liver microsomal incubation of JTT-130 (10 μM) conducted at 37 °C for 30 min in the presence of H<sub>2</sub><sup>18</sup>O (89.7%) did not reveal <sup>18</sup>O incorporation into the carboxylic acid metabolite **1** (Figure 8, panel A). <sup>18</sup>O incorporation, however, was noted in the atropic acid metabolite M2 (Figure 2S, Supporting Information) that was generated in the JTT-130/human liver microsomal incubations. Lack of <sup>18</sup>O incorporation in **1** suggested that the carboxylic acid metabolite is not formed by direct ester hydrolysis of JTT-130. Incorporation of <sup>18</sup>O in M2 served as an internal control for direct hydrolysis of the pendant ester group(s) in JTT-130. In contrast with the observations with JTT-130, human liver microsomal incubations with **3** in the

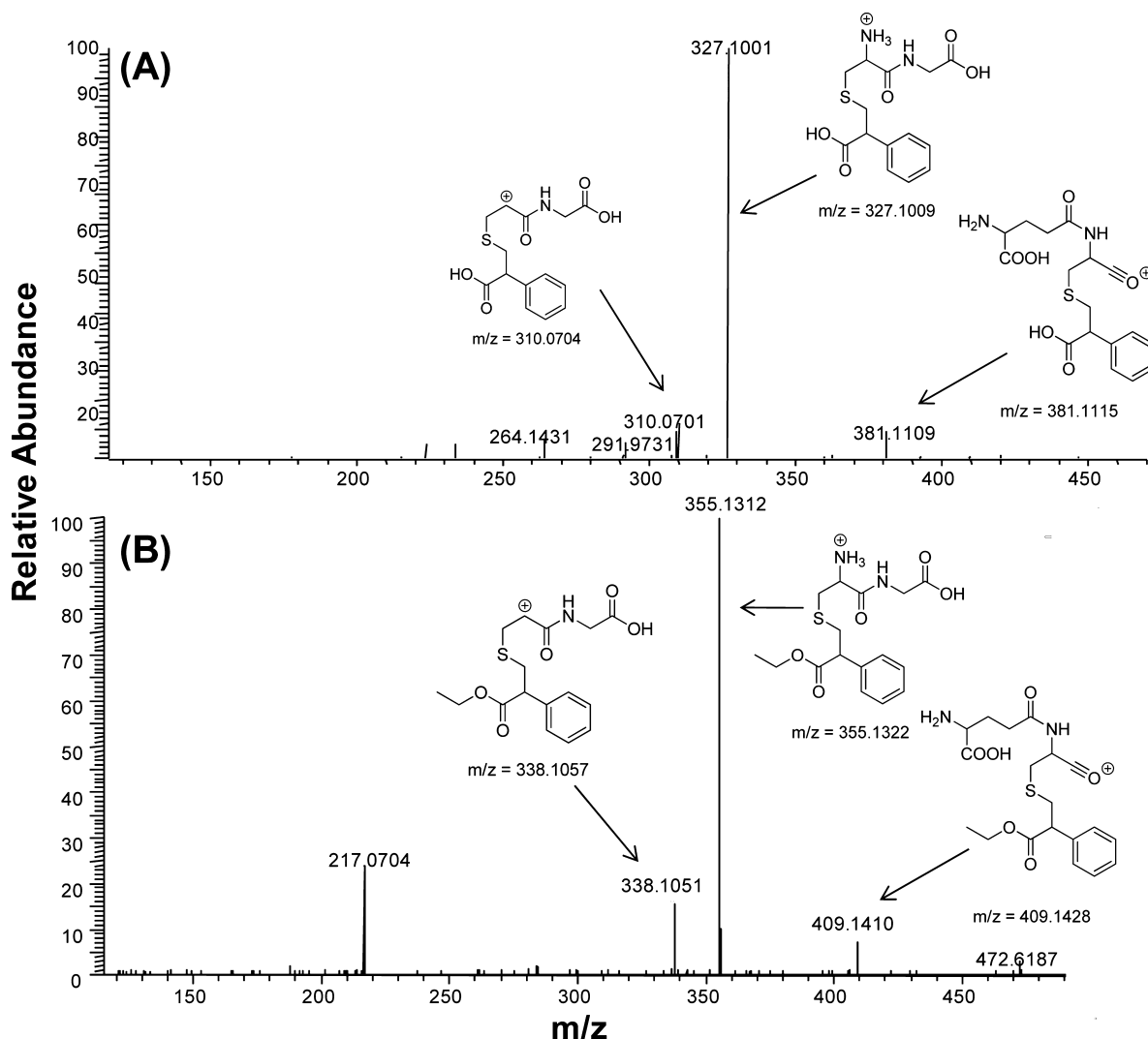


**Figure 10.** CID spectra of the glutathione conjugates of atropic acid (panel A) and its ethyl ester **5** (panel B).

presence of  $\text{H}_2^{18}\text{O}$  showed incorporation of  $^{18}\text{O}$  in **1** demonstrating direct ester hydrolysis of **3** (Figure 8, panel B).

**Reactive Metabolite Trapping Studies.** Human liver microsomal incubation of JTT-130 in the presence of exogenously added GSH indicated the formation of the GSH conjugates of atropic acid ( $t_R = 8.82$  min,  $\text{MH}^+$  at  $m/z$  456.1435) and its ethyl ester derivative **5** ( $t_R = 14.23$  min,  $\text{MH}^+$  at  $m/z$  484.1748) in trace quantities (Figure 9, panels A and B). The fragment ions at  $m/z$  327.1001 (Figure 10, panel A) and  $m/z$  355.1322 (Figure 10, panel B) in the CID spectra of the GSH conjugates of atropic acid and **5**, respectively, are derived from the characteristic loss of the pyroglutamic acid component of GSH.<sup>27</sup>

## DISCUSSION

The metabolism-guided approach leading to the discovery of JTT-130 constitutes an elegant tactic toward delivering a selective inhibitor of intestinal MTP.<sup>20</sup> JTT-130 was designed to be rapidly hydrolyzed and inactivated (to the carboxylic acid metabolite **1**) via hydrolytic cleavage of the ester group immediately after intestinal absorption. The success of this strategy is evident from the lack of elevated transaminase levels in phase I clinical trials with JTT-130. From a drug design perspective, it is likely that Mera et al.<sup>20</sup> capitalized on the known

differences in ester substrate specificities for the human serine esterases, carboxylesterase 1 (hCE-1), and carboxylesterase 2 (hCE-2), respectively. Although both hCE-1 and hCE-2 are present in several organs, the hydrolase activity of the liver and small intestine is predominantly attributed to hCE-1 and hCE-2, respectively.<sup>29,30</sup> Furthermore, the substrate specificity of hCE-1 and hCE-2 is significantly different; hCE-2 recognizes a substrate with a large alcohol group and small acyl group. In contrast, hCE-1 mainly hydrolyzes a substrate with a small alcohol group and large acyl group.<sup>29,30</sup> On the basis of the JTT-130 structure (the presence of a large acyl group and a small alcohol group), it is plausible that hydrolysis of JTT-130 to **1** in human liver microsomes is mediated by hCE-1. The finding that JTT-130 is resistant to hydrolytic cleavage ( $t_{1/2} > 90$  min) in human intestinal microsomes (Goosen, T., and Lapham K., unpublished observations) appears to corroborate this hypothesis.

Although the formation of **1** in JTT-130 incubations in human S-9 fractions has been previously noted, there is no information pertaining to the formation of the alcohol metabolite **2** in these incubations.<sup>20</sup> Our present work establishes that JTT-130 is not hydrolyzed in a straightforward fashion to yield carboxylic acid **1** and alcohol **2** as judged from the lack of incorporation of  $^{18}\text{O}$  in **1** in human liver microsomal incubations of JTT-130 in the presence of  $\text{H}_2^{18}\text{O}$ . We rationalize JTT-130 hydrolysis to proceed

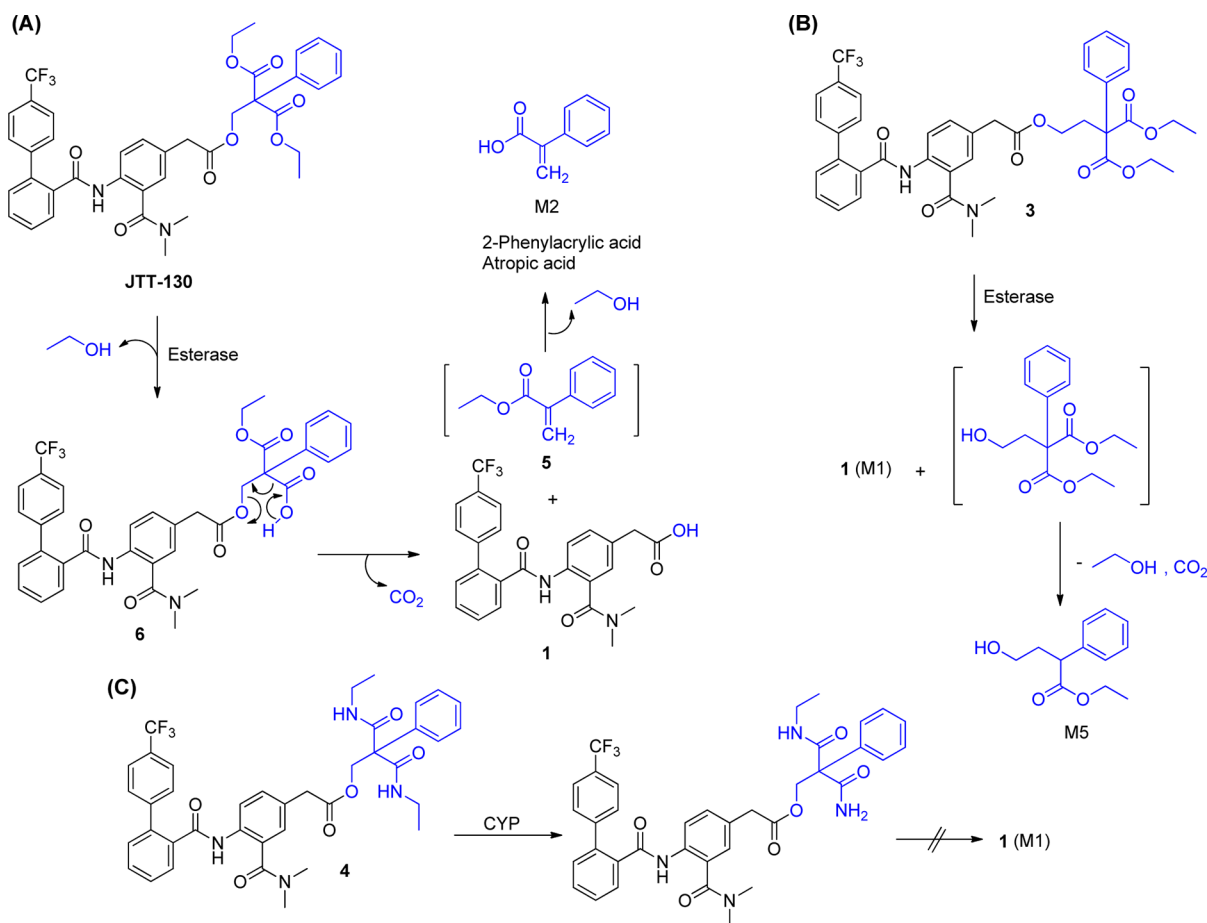


**Figure 11.** Mechanism of hydrolytic cleavage of JTT-130.

via the initial hydrolytic cleavage of one of the pendant malonic acid ethyl ester substituents to yield the carboxylic acid intermediate **6** that would spontaneously undergo decarboxylative fragmentation to yield **1** and the ethyl ester of atropic acid **5** (Figure 11, pathway A). Although **5** was not detected as a metabolite in the microsomal incubations with JTT-133, its formation was inferred from the characterization of the corresponding GSH adduct. Furthermore, the MS and NMR characterization of atropic acid, which can be obtained via the hydrolysis of **5** in the JTT-130/human liver microsomal incubations, provides additional credence to our theory.

To further test our hypothesis, compounds **3** and **4** were synthesized. Ester **3** possesses an additional methylene group on the alcohol substituent (diethyl 2-(2-hydroxyethyl)-2-phenylmalonate in **3** instead of diethyl 2-(hydroxymethyl)-2-phenylmalonate in JTT-130) and cannot undergo the decarboxylative fragmentation following hydrolysis of one of the pendant malonate ester groups. The formation of **1** from **3** can only arise through a direct hydrolysis of the ester linkage (Figure 11, pathway B), and this was reflected in the  $^{18}\text{O}$  incorporation in **1** following an incubation of **3** in microsomes in the presence of  $\text{H}_2^{18}\text{O}$ . Ester **4**, which incorporated an  $N^1, N^3$ -diethyl-2-phenylmalonamide substituent (instead of the diethyl-2-phenylmalonate motif in JTT-130) failed to generate **1** in human liver microsomes. Although the malonamide motif was deliberately incorporated to block decarboxylative elimination, we did not anticipate the complete resistance of **4** toward hydrolysis. This finding implies that the central ester linkage in **4** (and for that matter JTT-130) is sterically hindered and cannot undergo

hydrolytic cleavage by hCE-1. From a structure–activity relationship perspective, it is interesting to note that the mere addition of the extra methylene linker in **3** drastically lessens the steric hindrance around the central ester linkage thereby increasing its susceptibility toward hydrolytic cleavage. As such, these observations also highlight the importance of the pendant malonate ester groups in the efficient detoxication of JTT-130 to the inactive acid metabolite **1** in the liver.

From a toxicological perspective, it is tempting to draw parallels between the JTT-130 hydrolysis process resulting in the liberation of electrophilic  $\alpha,\beta$ -unsaturated carbonyl derivative (atropic acid and its corresponding ethyl ester **5**) byproduct and the bioactivation pathway proposed for the anticonvulsant felbamate, which is associated with significant incidences of aplastic anemia and hepatotoxicity.<sup>31,32</sup> The rate-limiting step in felbamate bioactivation (Figure 12) is believed to involve an amidase-mediated hydrolysis of one of the carbamate groups to 2-phenyl-1,3-propanediol monocarbamate (**7**), which is subsequently oxidized by alcohol dehydrogenase to 3-carbamoyl-2-phenylpropionaldehyde (**8**). Aldehyde **8**, which exists in equilibrium with the cyclized 4-hydroxy-5-phenyl-tetrahydro-1,3-oxazin-2-one (**9**) tautomer, is highly unstable ( $t_{1/2} < 30$  s) under physiological conditions and spontaneously degrades to the electrophilic 2-phenylpropenal (atropaldehyde, **10**) metabolite that adducts with GSH under nonenzymatic conditions (pH 7.4 buffer) and in the presence of glutathione transferases (Figure 12, pathway a).<sup>33–37</sup> In addition, GSH conjugates of atropic acid (also characterized as a metabolite of JTT-130) have been characterized in human liver S9 incubations with the

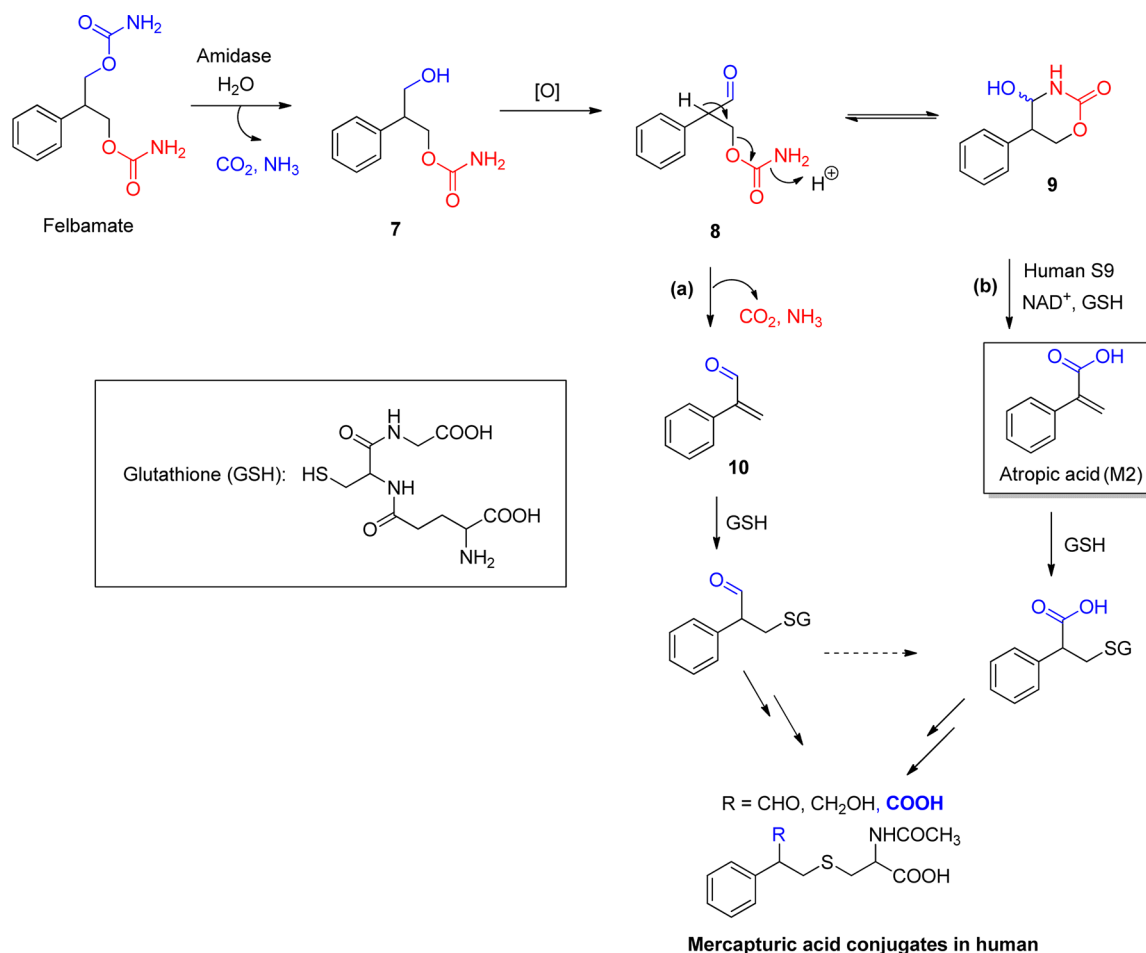


**Figure 12.** Bioactivation of the anticonvulsant felbamate to reactive species.

synthetic oxazin-2-one (9) metabolite of felbamate in the presence of  $\text{NAD}^+$  and GSH (Figure 12, pathway b).<sup>38</sup> *In vivo* evidence for the occurrence of these bioactivation pathways has been obtained via the characterization of urinary mercapturic acid conjugates of atropic acid (and its reduced alcohol form) following felbamate administration to rats and humans.<sup>33–35</sup> Whether the sulfhydryl conjugates of atropic acid observed *in vivo* are derived from direct conjugation of GSH to the  $\alpha,\beta$ -unsaturated carboxylic acid or through initial adduction with 10 followed by further oxidation to atropic acid remains unclear. As such, chemical reactivity studies with GSH reveal atropic acid to be a significantly weaker electrophile compared to atropaldehyde, although the role of glutathione transferases as catalysts of this reaction has yet to be explored.<sup>38</sup> Regardless of the differences in the relative Michael acceptor properties of the  $\alpha,\beta$ -unsaturated-aldehyde and -carboxylic acid, the formation of GSH conjugates of atropic acid and the corresponding ethyl ester 5 in the course of JTT-130 hydrolysis can be viewed as an undesirable feature from a toxicological perspective. The formation of GSH conjugate(s), an indicator of reactive species formation, is of particular concern due to the cumulative evidence supporting the hypothesis that reactive metabolites can be involved in direct organ toxicity as well as in idiosyncratic adverse drug reactions, leading to suspension from clinical trials, black box warnings, or, in some cases, withdrawal from the market.<sup>39</sup> The potential for idiosyncratic immune-mediated toxicity arising through adduction of atropic acid or the ethyl ester 5 to proteins is too high of a risk, especially in a disease area with diverse

therapeutic options (e.g., statins and fibrates). In conclusion, the mechanistic insights gathered from the present work on JTT-130 hydrolysis can be potentially utilized in the design of ester-based gut MTP inhibitors that are incapable of yielding the electrophilic acrylate species upon hydrolysis in the liver.

## ■ ASSOCIATED CONTENT

### ● Supporting Information

CID spectrum for the carboxylic acid metabolite (M1) and extracted ion chromatograms depicting  $^{18}\text{O}$  incorporation in the atropic acid metabolite obtained upon incubation of JTT-130 in human liver microsomes. This material is available free of charge via the Internet at <http://pubs.acs.org>.

## ■ AUTHOR INFORMATION

### Corresponding Author

\*Tel: (617)-551-3336. E-mail: [amit.kalgutkar@pfizer.com](mailto:amit.kalgutkar@pfizer.com).

### Notes

The authors declare no competing financial interest.

## ■ ABBREVIATIONS

MTP, microsomal triglyceride transfer protein; TG, triglyceride; VLDL, very low density lipoprotein; JTT-130, diethyl 2-((2-(3-(dimethylcarbamoyl)-4-(4'-(trifluoromethyl)-[1,1'-biphenyl]-2-ylcarboxamido)phenyl)acetoxy)methyl)-2-phenylmalonate; 1, 2-(3-(dimethylcarbamoyl)-4-(4'-(trifluoromethyl)-[1,1'-biphenyl]-2-ylcarboxamido)phenyl)acetic acid; 2, diethyl



2-(hydroxymethyl)-2-phenyl malonate; **3**, diethyl 2-(2-(3-(dimethylcarbamoyl)-4-(4'-trifluoromethyl)-[1,1'-biphenyl]-2-ylcarboxamido)phenyl)acetoxyethyl)-2-phenylmalonate; **4**, 3-(ethylamino)-2-(ethylcarbamoyl)-3-oxo-2-phenylpropyl 2-(3-(dimethylcarbamoyl)-4-(4'-(trifluoromethyl)-[1,1'-biphenyl]-2-ylcarboxamido)phenyl)acetate; *J*, coupling constant; ESI, electrospray ionization; GSH, glutathione; P450, cytochrome P450; LC-MS/MS, liquid chromatography tandem mass spectrometry;  $t_{1/2}$ , half-life;  $t_R$ , retention time; CID, collision-induced dissociation; HSQC, multiplicity edited heteronuclear single quantum coherence; HMBC, heteronuclear multiple bond correlation; hCE-1, human carboxylesterase-1; hCE-2, human carboxylesterase-2

## REFERENCES

- (1) Jamil, H., Dickson, J. K., Jr., Chu, C. H., Lago, M. W., Rinehart, J. K., Biller, S. A., Greg, R. E., and Wetterau, J. R. (1995) Microsomal triglyceride transfer protein. Specificity of lipid binding and transport. *J. Biol. Chem.* 270, 6549–6554.
- (2) Burnett, J. R., and Watts, G. F. (2007) MTP inhibition as a treatment for dyslipidaemias: time to deliver or empty promises. *Expert Opin. Ther. Targets* 11, 181–189.
- (3) Wetterau, J. R., Aggerbeck, L. R., Bouma, M. E., Eisenberg, C., Munck, A., Hermier, M., Schmitz, J., Gay, G., Rader, D. J., and Gregg, R. E. (1992) Absence of microsomal triglyceride transfer protein in individuals with abetalipoproteinemia. *Science* 258, 999–1001.
- (4) Sharp, D., Blinderman, L., Combs, K. A., Kienzie, B., Ricci, B., Wager-Smith, K., Gil, C. M., Turck, C. W., Bouma, M. E., Rader, D. J., Aggerbeck, L. P., Gregg, R. E., Gordon, D. A., and Wetterau, J. R. (1993) Cloning and gene defects in microsomal triglyceride transfer protein associated with abetalipoproteinemia. *Nature* 365, 65–69.
- (5) Rader, D. J., and Brewer, H. B. (1993) Abetalipoproteinemia. New insights into lipoprotein assembly and vitamin E metabolism from a rare genetic disease. *JAMA* 270, 865–869.
- (6) Liao, W., Hui, T. Y., Young, S. G., and Davis, R. A. (2003) Blocking microsomal triglyceride transfer protein interferes with apoB secretion without causing retention or stress in the ER. *J. Lipid Res.* 44, 978–985.
- (7) Wetterau, J. R., Gregg, R. E., Harrity, T. W., Arbeen, C., Cap, M., Connolly, F., Chu, C. H., George, R. J., Gordon, D. A., Jamil, H., Jolibois, K. G., Kunselman, L. K., Lan, S. J., Maccagnan, T. J., Ricci, B., Yan, M., Young, D., Chen, Y., Fryszman, O. M., Logan, J. V., Musial, C. L., Poss, M. A., Robl, J. A., Simpkins, L. M., Slusarchyk, W. A., Sulsky, R., Taunk, P., Magnin, D. R., Tino, J. A., Lawrence, R. M., Dickson, J. K., Jr., and Biller, S. A. (1998) An MTP inhibitor that normalizes atherogenic lipoprotein levels in WHHL rabbits. *Science* 282, 751–754.
- (8) Chandler, C. E., Wilder, D. E., Pettini, J. L., Savoy, Y. E., Petras, S. F., Chang, G., Vincent, J., and Harwood, H. J., Jr. (2003) CP-346086: an MTP inhibitor that lowers plasma cholesterol and triglycerides in experimental animals and in humans. *J. Lipid Res.* 44, 1887–1901.
- (9) Cuchel, M., Bloedon, L. T., Szapary, P. O., Kolansky, D. M., Wolfe, M. L., Sarkis, A., Millar, J. S., Ikewaki, K., Siegelman, E. S., Greg, R. E., and Rader, D. J. (2007) Inhibition of microsomal triglyceride transfer protein in familial hypercholesterolemia. *N. Engl. J. Med.* 356, 148–156.
- (10) Miyazaki, Miwa, S., Kodama, H., Yamada, H., Nagata, K., Toriumi, W., Kitamura, K., and Kume, E. (2007) Hepatic and intestinal changes in rats treated with T-0126, a microsomal triglyceride transfer protein (MTP) inhibitor. *J. Toxicol. Sci.* 32, 161–177.
- (11) Samaha, F. F., McKenney, J., Bloedon, L. T., Sasiela, W. J., and Rader, D. J. (2008) Inhibition of microsomal triglyceride transfer protein alone or with ezetimibe in patients with moderate hypercholesterolemia. *Nat. Clin. Pract. Cardiovasc. Med.* 5, 497–505.
- (12) Rizzo, M., and Wierzbicki, A. S. (2011) New lipid modulating drugs: the role of microsomal transport protein inhibitors. *Curr. Pharm. Des.* 17, 943–949.
- (13) Rizzo, M. (2010) Lomitapide, a microsomal triglyceride transfer protein inhibitor for the treatment of hypercholesterolemia. *IDrugs* 13, 103–111.
- (14) Gambino, R., Cassader, M., Pagano, G., Durazzo, M., and Musso, G. (2007) Polymorphism in microsomal triglyceride transfer protein: a link between liver disease and atherogenic postprandial lipid profile in NASH? *Hepatology* 45, 1097–1107.
- (15) Bernard, S., Touzet, S., Personne, I., Lapras, V., Bondon, P. J., Berthezene, F., and Moulin, P. (2000) Association between microsomal triglyceride transfer protein gene polymorphism and the biological features of liver steatosis in patients with type II diabetes. *Diabetologia* 43, 995–999.
- (16) Wierzbicki, A. S., Hardman, T., and Prince, W. T. (2009) Future challenges for microsomal transport protein inhibitors. *Curr. Vasc. Pharmacol.* 7, 277–286.
- (17) Vu, C. B., Milne, J. C., Carney, D. P., Song, J., Choy, W., Lambert, P. D., Gagne, D. J., Hirsch, M., Cote, A., Davis, M., Lainez, E., Meade, N., Normington, K., Jirousek, M. R., and Perni, R. B. (2009) Discovery of benzothiazole derivatives as efficacious and enterocyte-specific MTP inhibitors. *Bioorg. Med. Chem. Lett.* 19, 1416–1420.
- (18) Kim, E., Campbell, S., Schueller, O., Wong, E., Cole, B., Kuo, J., Ellis, J., Ferkany, J., and Sweetnam, P. (2011) A small-molecule inhibitor of enterocytic microsomal triglyceride transfer protein, SLX-4090: biochemical, pharmacodynamic, pharmacokinetic, and safety profile. *J. Pharmacol. Exp. Ther.* 337, 775–785.
- (19) Raval, S. K., Raval, P. S., and Jain, M. R. (2012) Emerging therapies for dyslipidemia: known knowns and known unknowns of MTP inhibitors. *Recent Pat. Endocr. Metab. Immune Drug Discovery* 6, 24–29.
- (20) Mera, Y., Odani, N., Kawai, T., Hata, T., Suzuki, M., Hagiwara, A., Katsushima, T., and Kakutani, M. (2011) Pharmacological characterization of diethyl-2-[(3-dimethylcarbamoyl-4-[(4'-trifluoromethylbiphenyl-2-carbonyl)amino]phenyl)acetyloxymethyl]-2-phenylmalonate (JTT-130), an intestine-specific inhibitor of microsomal triglyceride transfer protein. *J. Pharmacol. Exp. Ther.* 336, 321–327.
- (21) Hata, T., Mera, Y., Ishii, Y., Tadaki, H., Tomimoto, D., Kuroki, Y., Kawai, T., Ohta, T., and Kakutani, M. (2011) JTT-130, a novel intestine-specific inhibitor of microsomal triglyceride transfer protein, suppresses food intake and gastric emptying with the elevation of plasma peptide YY and glucagon-like peptide-1 in a dietary fat-dependent manner. *J. Pharmacol. Exp. Ther.* 336, 850–856.
- (22) Hata, T., Mera, Y., Tadaki, H., Kuroki, Y., Kawai, T., Ohta, T., and Kakutani, M. (2011) JTT-130, a novel intestine-specific inhibitor of microsomal triglyceride transfer protein, suppresses high fat diet-induced obesity and glucose intolerance in Sprague-Dawley rat. *Diabetes Obes. Metab.* 13, 446–454.
- (23) Hata, T., Mera, Y., Kawai, T., Ishii, Y., Kuroki, Y., Kakimoto, K., Ohta, T., and Kakutani, M. (2011) JTT-130, a novel intestine-specific inhibitor of microsomal triglyceride transfer protein, ameliorates impaired glucose and lipid metabolism in Zucker diabetic fatty rats. *Diabetes Obes. Metab.* 13, 629–638.
- (24) Li, J., Bronk, B. S., Dirlam, J. P., Blize, A. E., Bertinato, P., Jaynes, B. H., Hickman, A., Miskell, C., Pillai, U. A., Tibbitts, J. S., Haven, M. L., Kolosko, N. L., Barry, C. J., and Manion, T. B. (2007) In vitro and in vivo profile of 5-[(4'-trifluoromethyl-biphenyl-2-carbonyl)-amino]-1H-indole-2-carboxylic acid benzylmethyl carbamoylamide (dirlotapide), a novel potent MTP inhibitor for obesity. *Bioorg. Med. Chem. Lett.* 17, 1996–1999.
- (25) Robinson, R. P., Bartlett, J. A., Bertinato, P., Bessire, A. J., Cosgrove, J., Foley, P. M., Manion, T. B., Minich, M. L., Ramos, B., Reese, M. R., Schmahai, T. J., Swick, A. G., Tess, D. A., Vaz, A., and Welford, A. (2011) Discovery of microsomal triglyceride transfer protein (MTP) inhibitors with potential for decreased active metabolite load compared to dirlotapide. *Bioorg. Med. Chem. Lett.* 21, 4150–4154.
- (26) Hagiwara, A., Yasuhiro, O., Odani, N., Watanabe, S., Ikenogami, T., Kawai, T., Madono, K., Taniguchi, T. (2009) Ester Compound and Medicinal Use Thereof, US7625948.
- (27) Baillie, T. A., and Davis, M. R. (1993) Mass spectrometry in the analysis of glutathione conjugates. *Biol. Mass Spectrom.* 22, 319–325.
- (28) Kim, H. I., and Beauchamp, J. L. (2007) Cluster phase chemistry: collisions of vibrationally excited cationic dicarboxylic acid clusters with

water molecules initiate dissociation of cluster components. *J. Phys. Chem. A* 111, 5954–5967.

(29) Imai, T. (2006) Human carboxylesterase isozymes: catalytic properties and rational drug design. *Drug Metab. Pharmacokinet.* 21, 173–185.

(30) Satoh, T., Taylor, P., Bosron, W. F., Sanghani, S. P., Hosokawa, M., and La Du, B. N. (2002) Current progress on esterases: from molecular structure to function. *Drug Metab. Dispos.* 30, 488–493.

(31) Nightingale, S. L. (1994) From the food and drug administration. *JAMA* 272, 995.

(32) Pellock, J. M. (1999) Felbamate in epilepsy therapy: evaluating the risks. *Drug Saf.* 21, 225–239.

(33) Thompson, C. D., Gulden, P. H., and Macdonald, T. L. (1997) Identification of modified atropaldehyde mercapturic acids in rat and human urine after felbamate administration. *Chem. Res. Toxicol.* 10, 457–462.

(34) Thompson, C. D., Barthen, M. T., Hopper, D. W., Miller, T. A., Quigg, M., Hudspeth, C., Montouris, G., Marsh, L., Perhach, J. L., Sofia, R. D., and Macdonald, T. L. (1999) Quantification in patient urine samples of felbamate and three metabolites: acid carbamate and two mercapturic acids. *Epilepsia* 40, 769–776.

(35) Dieckhaus, C. M., Thompson, C. D., Roller, S. G., and MacDonald, T. L. (2002) Mechanisms of idiosyncratic drug reactions: the case of felbamate. *Chem.-Biol. Interact.* 142, 99–117.

(36) Dieckhaus, C. M., Roller, S. G., Santos, W. L., Sofia, R. D., and Macdonald, T. L. (2001) Role of glutathione S-transferases A1–1, M1–1, and P1–1 in the detoxification of 2-phenylpropenal, a reactive felbamate metabolite. *Chem. Res. Toxicol.* 14, 511–516.

(37) Adusumalli, V. E., Choi, Y. M., Romanyshyn, L. A., Sparadoski, R. E., Jr., Wichmann, J. K., Wong, K. K., Kucharczyk, N., and Sofia, R. D. (1993) Isolation and identification of 3-carbamoyloxy-2-phenylpropionic acid as a major human urinary metabolite of felbamate. *Drug Metab. Dispos.* 21, 710–716.

(38) Parker, R. J., Hartman, N. R., Roecklein, B. A., Mortko, H., Kupferberg, H. J., Stables, J., and Strong, J. M. (2005) Stability and comparative metabolism of selected felbamate metabolites and postulated fluorofelbamate metabolites by postmitochondrial suspensions. *Chem. Res. Toxicol.* 18, 1842–1848.

(39) Stepan, A. F., Walker, D. P., Bauman, J., Price, D. A., Baillie, T. A., Kalgutkar, A. S., and Aleo, M. D. (2011) Structural alert/reactive metabolite concept as applied in medicinal chemistry to mitigate the risk of idiosyncratic drug toxicity: a perspective based on the critical examination of trends in the top 200 drugs marketed in the United States. *Chem. Res. Toxicol.* 24, 1345–1410.